Evidence for an Intramolecular Charge Transfer State in 12′-Apo-β-caroten-12′-al and 8′-Apo-β-caroten-8′-al: Influence of Solvent Polarity and Temperature

Matthäus Kopczynski, Florian Ehlers, Thomas Lenzer,* and Kawon Oum*

Institut für Physikalische Chemie, Universität Göttingen, Tammannstrasse 6, D-37077 Göttingen, Germany

Received: November 2, 2006; In Final Form: March 24, 2007

The ultrafast excited-state dynamics of two carbonyl-containing carotenoids, 12′-apo-β-caroten-12′-al and 8′-apo-β-caroten-8′-al, have been investigated by transient absorption spectroscopy in a systematic variation of solvent polarity and temperature. In most of the experiments, 12′-apo-β-caroten-12′-al was excited at 430 nm and 8′-apo-β-caroten-8′-al at 445 or 450 nm via the $S_0 \rightarrow S_2$ ($1^1A_g^- \rightarrow 1^1B_u^+$) transition. The excited-state dynamics were then probed at 860 nm for 12′-apo-β-caroten-12′-al and at 890 or 900 nm for 8′-apo-β-caroten-8′-al. The temporal evolution of all transient signals measured in this work can be characterized by an ultrafast decay of the $S_2 \rightarrow S_N$ absorption at early times followed by the formation of a stimulated emission (SE) signal, which subsequently decays on a much slower time scale. We assign the SE signal to a low-lying electronic state of the apocarotenals with intramolecular charge-transfer character (ICT $\rightarrow S_0$). This is the first time that the involvement of an ICT state has been detected in the excited-state dynamics of a carbonyl carotenoid in nonpolar solvents such as *n*-hexane or *i*-octane. The amplitude ratio of ICT-stimulated emission to S_2 absorption was weaker in nonpolar solvents than in polar solvents. We interpret the results in terms of a kinetic model, where the S_1 and ICT states are populated from S_2 through an ultrafast excited-state branching reaction ($\tau_2 < 120$ fs). Delayed formation of a part of the stimulated emission is due to the transition $S_1 \rightarrow$ ICT ($\tau_3 = 0.5-4.1$ ps, depending on the solvent), which possibly involves a slower backward reaction ICT $\rightarrow S_1$. Determinations of τ_1 were carried out for a large set of solvents. Especially in 12′-apo-β-caroten-12′-al, the final SE decay, assigned to the nonradiative relaxation ICT $\rightarrow S_0$, was strongly dependent on solvent polarity, varying from $\tau_1 = 200$ ps in *n*-hexane to 6.6 ps in methanol. In the case of 8′-apo-β-caroten-8′-al, corresponding values were 24.8 and 7.6 ps, respectively. This indicates an increasing stabilization of the ICT state with increasing solvent polarity, resulting in a decreasing ICT−S_0 energy gap. Tuning the pump wavelength from the blue wing to the maximum of the $S_0 \rightarrow S_2$ absorption band resulted in no change of τ_1 in acetone and methanol. Additional measurements in methanol after excitation in the red edge of the $S_0 \rightarrow S_2$ band (480−525 nm) also show an almost constant τ_1 with only a 10% reduction at the largest probe wavelengths. The temperature dependence of the τ_1 value of 12′-apo-β-caroten-12′-al was well described by Arrhenius-type behavior. The extracted apparent activation energies for the ICT $\rightarrow S_0$ transitions were in general small (on the order of a few times *RT*), which is in the range expected for a radiationless process.

1. Introduction

Understanding the energy, structure, and dynamics of the excited electronic states of carotenoids is the key step to characterize their role as light-harvesting (LH) and photoprotective pigments after they absorb light in the spectral region between 400 and 550 nm.[1,2] The route and the efficiency of energy transfer between carotenoids and (bacterio)chlorophyll [(B)Chl] in LH complexes depend strongly on the lifetimes of their first few excited singlet states.

If C_{2h} symmetry is assumed for its polyene backbone, theoretical calculations[3,4] predict $1^1A_g^-$ symmetry for the ground state (S_0) of the carotenoid and the presence of several low-lying singlet-excited states including $2^1A_g^-$, $1^1B_u^+$, $1^1B_u^-$, $3^1A_g^-$, $1^1A_g^+$, and $4^1A_g^-$. $2^1A_g^-$ is the lowest singlet excited state and is known as the S_1 state. The relative energy levels of the other states depend on the number of conjugated double bonds.[3] Among these states, the transition to the $1^1B_u^+$ state (S_2 state) is optically active and other states are symmetry-forbidden for a one-photon transition. Direct experimental identification of the dark states, denoted as $1^1B_u^-$, $3^1A_g^-$,[5,6] S_x,[7] S^*,[8−12] or $S^‡$,[13] and their role in relaxation pathways of excited carotenoids is still under debate.[2,14]

Upon excitation to the S_2 state, the main features of the radiationless deactivation route of excited carotenoids are typically described by a simplified three-state model ($S_2 \rightarrow S_1 \rightarrow S_0$), that is, the first fast internal conversion step $S_2 \rightarrow S_1$, on the time scale 50−300 fs, is followed by the second considerably slower internal conversion $S_1 \rightarrow S_0$, in the range of a few to a few hundred picoseconds. Since Wasielewski and Kispert reported the first measurement of the S_1 lifetimes of carotenoids (β-carotene, canthaxanthin, and 8′-apo-β-caroten-8′-al) in 1986,[15] the S_1 dynamics of other carotenoids have been extensively studied by several research groups with respect to their dependence on the conjugation length, solvent polarity, excitation wavelength, terminal groups, etc. (see, for example, the review by Polívka and Sundström[2] and references cited therein). First, it is now well-established that the S_1 lifetime of unsubstituted carotenoids depends primarily on the polyene chain length.[16] Second, especially in relation to the present work,

* Corresponding authors: tel +49 551 3912598; fax +49 551 393150, e-mail tlenzer@gwdg.de (T.L.) or koum@gwdg.de (K.O.).

10.1021/jp0672252 CCC: $37.00
Published on Web 06/06/2007

the S_1 lifetimes of C_{40} carotenoids [such as β-carotene, lycopene, (3*R*,3′*R*)-zeaxanthin, (3*R*,3′*R*,6′*R*)-lutein, and the keto carotenoids echinenone, canthaxanthin and astaxanthin] were found to be independent of solvent polarity.[17] Third, with respect to the "fast" relaxation pathways after excitation to the S_2 state, even more interesting and elaborate interpretations have been suggested, mainly based on the findings of excitation wavelength-dependent transient absorption studies, which cannot be easily explained by the simplified three-state model ($S_2 \rightarrow S_1 \rightarrow S_0$). For example, when zeaxanthin was excited at shorter wavelengths into higher vibrational bands of the S_2 state, Billsten et al.[11] detected an increase of the absorption band near 510 nm which was assigned to the S* state, which had been also observed before.[8−10,12] In this case, excitation to higher vibrational states of S_2 may also open new relaxation channels, such as S_2(hot) → S*. Additional time constants of 2.8 ps (400 nm excitation) and 4.9 ps (266 nm excitation) were necessary to describe the relaxation kinetics, whereas no additional time constant was required after 485 nm excitation into the lowest vibrational band of the S_2 state. Billsten et al.[11] interpret this additional kinetic component as a conformational relaxation process due to the excess energy excitation, such that the larger the excess excitation energy the longer it takes to restore the fully relaxed S_1 state. It should be noted that this complexity due to the excitation wavelength dependence, however, does not affect the lifetimes of the S_1 state.[11]

When carotenoids contain electron-withdrawing substituents, such as cyano groups in 7′,7′-dicyano-7′-apo-β-carotene or a carbonyl group in peridinin, 12′-apo-β-caroten-12′-al, and 8′-apo-β-caroten-8′-al, the relaxation process becomes more complicated. The lifetime of S_1 strongly depends on the solvent polarity: for example, in 12′-apo-β-caroten-12′-al, S_1 lifetimes of 220 and 8 ps were measured in *n*-hexane and methanol, respectively.[18] He et al.[16] determined S_1 lifetimes of selected carotenoids having different terminal groups, like -CN, -CO_2-Et, and -CHO, and found out that carotenoids with terminal -CHO groups have a smaller S_1 lifetime in polar solvents, while other terminal groups have little effect. Solvent-dependent S_1 lifetimes were, however, observed for 7′,7′-dicyano-7′-apo-β-carotene.[16,19] Notable progress in understanding the excited states dynamics of carbonyl carotenoids has been made on the basis of extensive studies of peridinin and the peridinin−chlorophyll *a*−protein (PCP) complex. For peridinin itself, a lifetime of ∼160 ps was observed in nonpolar solvents, whereas the lifetime was as short as 10 ps in methanol.[20−22] This solvent-dependent lifetime of peridinin has been attributed to the presence of an intramolecular charge transfer (ICT) state.[20−27] An important spectral fingerprint to support the presence of an ICT state was the observation of stimulated emission in the wavelength range 750−1400 nm in methanol, which was, however, not visible in *n*-hexane.[21,22] Absorption profiles recorded in the ICT band showed additional dynamics assigned to a rise-time component in the range 0.4−1.5 ps depending on the excitation wavelength, which was attributed to the formation or relaxation of the hot ICT state. Additional experimental evidence supporting the existence of an ICT state has been obtained by van Grondelle and co-workers[26,27] in their ultrafast dispersed pump−dump−probe and pump−repump−probe spectroscopic studies of peridinin in methanol in the visible region: A time-delayed 800 nm laser pulse preferentially and immediately dumped the stimulated emission and removed the ICT contribution. Furthermore, evidence for a re-equilibration between the S_1 and ICT states after dumping of the ICT population has been found. So far there is no doubt about the presence of ICT character in peridinin excited-state dynamics; however, the question remains whether the S_1 state itself has charge-transfer character,[25] or if there is a polarity-dependent mixing between S_1 and ICT states forming a combined S_1/ICT state with varying degree of ICT character,[22] or if there is a distinct ICT state clearly separated from[24] or in a fast equilibrium with the S_1 state.[26,27] Another important question in peridinin's excited-state dynamics is the role of dark states such as S* revealed by experimental results of the dependence on wavelength and intensity of the excitation pulse. Further open questions include the identification and the role of ground-state conformers and possible experimental complications due to two-photon excitation opening additional relaxation pathways.[22,27]

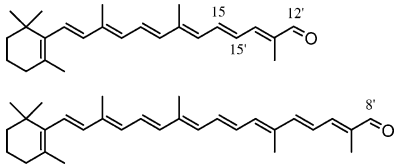

Figure 1. Chemical structures of 12′-apo-β-caroten-12′-al (top) and 8′-apo-β-caroten-8′-al (bottom).

In our previous transient absorption studies we have found that 12′-apo-β-caroten-12′-al, an aldehyde-substituted apocarotenoid (Figure 1, top), shows a strong solvent dependence of the S_1 lifetime (220 ps in *n*-hexane and 8 ps in methanol).[18] This is even stronger than that of peridinin. Such unusual behavior again points toward the presence of considerable ICT contributions in polar solvents. Therefore, we have started extensive experimental investigations of apocarotenal systems, which hopefully yield valuable information on the dynamics of carotenoids with ICT states in general and can also be helpful for the understanding of the excited-state dynamics of peridinin. In this work, we focus on the identification of the ICT state in 12′-apo-β-caroten-12′-al and 8′-apo-β-caroten-8′-al (a very similar system with longer conjugation length; see Figure 1, bottom) by detecting the time-resolved ICT stimulated emission as a function of solvent polarity and temperature. This will lead us to a better understanding of the role of the ICT state in the excited-state dynamics of these two carbonyl carotenoids.

2. Experimental Section

A mode-locked Ti:sapphire laser (Spectra-Physics Tsunami) pumped by a Nd:YVO_4 laser (Spectra-Physics Millenia Xs) was used to generate pulses between 740 and 900 nm with a repetition rate of 82 MHz and an average laser power of about 1.0−1.5 W. A dichroic mirror was used to split the laser beam into two parts. One part passed through an acousto-optic modulator (AOM, operating at a frequency of 2 MHz provided by a pulse generator) and was subsequently frequency-doubled in a LBO crystal to generate an intensity-modulated pump beam (370−450 nm) with pulse energies <0.1 nJ. The other part was used as probe beam, which had a typical energy <1 nJ $pulse^{-1}$ and was time-delayed with respect to the pump beam by means of a motorized computer-controlled delay line. The time resolution was typically about 120 fs, as estimated from optical Kerr lens (OKL) pump−probe signals[28] generated in a 1 mm thick quartz plate. The pump and probe pulses were recombined in a collinear beam-in-beam arrangement, with the polarization set to the magic angle to avoid any contributions from orientational relaxation effects. The pulses were then sent through a quartz lens (Suprasil I, $f = 50$ mm) and mildly focused into a quartz flow-through cuvette mounted on a linear translation stage, which contained the apocarotenal solution. Its entrance window surface was aligned perpendicularly with

respect to the incoming beams. A convex quartz lens (focal length 30 mm) was located behind the cuvette such that the probe beam was focused onto an avalanche photodiode. The pump beam was cut off in front of the photodiode by an appropriate combination of color and neutral density filters, so that the recorded intensity change was due only to the time-dependent absorption/stimulated emission of the sample detected by the probe beam. The resulting signal was fed into a lock-in amplifier that used the 2 MHz modulation of the pulse generator as its reference signal. The lock-in-signal was then transferred to a PC, which handled the signal acquisition by use of an A/D converter card and the control of the delay line via a GPIB interface by means of an Agilent VEE program.

The temperature-dependent experiments were carried out in a newly constructed cell that can be heated or cooled over the temperature range 263−353 K by flowing a temperature-controlled mixture of water and ethylene glycol through capillaries embedded in the cell body. The cell windows were made of quartz with a thickness of 1 mm, and the path length was adjustable in the range 1−2 mm. In the middle of the cell, a motor-driven stirrer was installed in order to remove unwanted effects due to thermal lensing and sample degradation.

The amplitude of the transient absorption/stimulated emission signals was linearly increasing with respect to the laser intensity of both pump and probe beams. This was checked over the range 1−10 mW (0.01−0.1 nJ pulse^{-1}) for the pump beam and 5−50 mW (0.06−0.6 nJ pulse^{-1}) for the probe beam. The pulse energies employed in our study were extremely low in order to avoid unwanted effects due to two-photon or multiphoton processes.

Complementing transient absorption signals of 12′-apo-β-caroten-12′-al in methanol were recorded at a probe wavelength of 390 nm with the ultrafast laser setup described in detail in ref 18 to further investigate its intramolecular dynamics after excitation on the red edge of the $S_0 \rightarrow S_2$ by using pump wavelengths between 480 and 525 nm.

The highly purified carotenoid samples were generously provided by BASF AG. 12′-Apo-β-caroten-12′-al and 8′-apo-β-caroten-8′-al were all in their *all-trans* (*all-E*) configuration with a purity >97%. All solvents had purity ≥99%. The typical concentration of the carotenoid was about 2×10^{-4} M, which was low enough to avoid aggregation. Steady-state absorption and fluorescence spectra were recorded on Varian Cary 5E and Horiba Jobin Yvon FluoroLog-3 spectrometers, respectively.

3. Results

Steady-State Absorption Spectra. Room-temperature steady-state absorption spectra of 12′-apo-β-caroten-12′-al and 8′-apo-β-caroten-8′-al in various solvents used in this work are shown in Figures 2 and 3, respectively. The strong absorption band in the range 350−550 nm is known to be associated with the $S_0(1^1A_g^-) \rightarrow S_2(1^1B_u^+)$ transition. The vibronic structure, absorption maxima, and full width at half-maximum (fwhm) of this absorption band were found to depend strongly on the solvent properties. In Figure 2, we arrange the absorption spectra in three groups of solvents: (A) nonpolar, (B) polar aprotic, and (C) polar protic. First of all, the vibronic structure of 12′-apo-β-caroten-12′-al is still visible in nonpolar solvents as shoulders; however, it disappears in polar solvents. In Figure 2A, a larger shift of the maximum peak position to longer wavelengths in solvents with stronger polarizability is clearly seen for nonpolar solvents. This solvent-induced spectral shift can be correlated with the Lorentz-Lorenz function $R(n) = (n^2 - 1)/(n^2 + 2)$, where n is the refractive index of the solvent.[29]

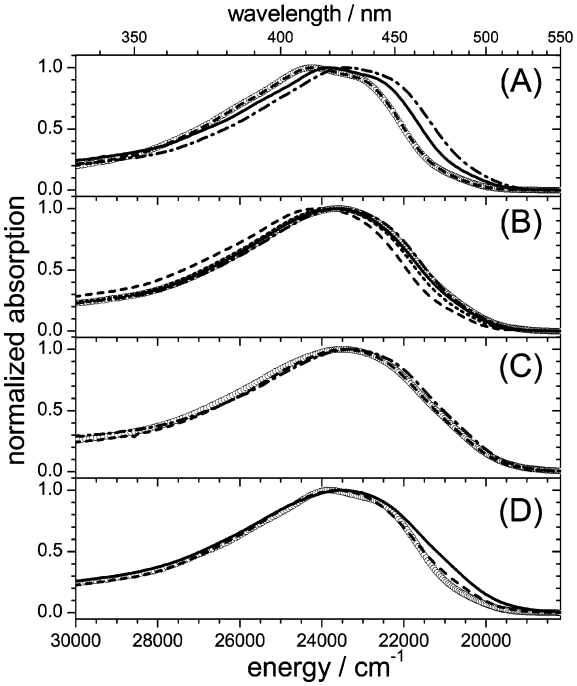

Figure 2. $S_0 \rightarrow S_2$ steady-state absorption spectra of 12′-apo-β-caroten-12′-al in various solvents at room temperature. The energy axis is shown in units of reciprocal centimeters, and the wavelength scale (in nanometers) is shown on top as a reference. (A) Nonpolar solvents in the order of increasing polarizability: (○) *n*-hexane, (---) *i*-octane, (—) cyclohexene, and (− · −) toluene. (B) Polar aprotic solvents: (---) diethyl ether, (···) ethyl acetate, (—) acetone, (○) acetonitrile, and (− · −) tetrahydrofuran. (C) Polar protic solvents: (○) methanol, (---) ethanol, and (− · −) *n*-butanol. (D) Comparison: (○) cyclohexene, (---) acetonitrile, and (—) methanol.

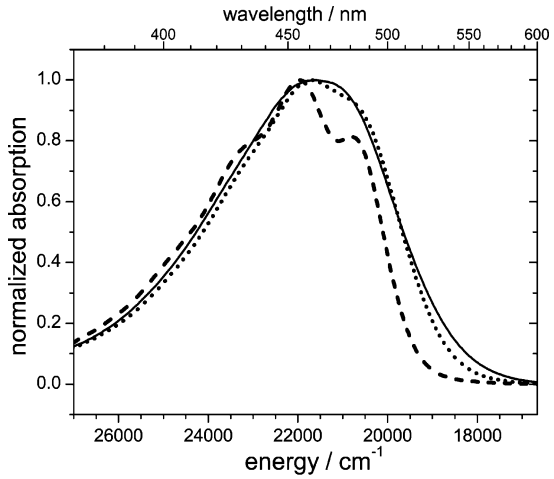

Figure 3. Examples of $S_0 \rightarrow S_2$ steady-state absorption spectra of 8′-apo-β-caroten-8′-al at room temperature in *i*-octane (---), acetonitrile (···), and methanol (—). Spectra are shown as a function of energy in reciprocal centimeters, and the wavelength scale (in nanometers) is given on top as a reference.

In the case of 12′-apo-β-caroten-12′-al and 8′-apo-β-caroten-8′-al in polar solvents, however, it is more complicated to correlate the apparent absorption maxima with respect to the vibronic transitions because of the lack of vibronic band structure, and therefore, we cannot simply compare the peak maxima in nonpolar solvents with those in polar solvents. Furthermore, the $S_0 \rightarrow S_2$ absorption band becomes broader in nonpolar solvents in the order *n*-hexane ≈ *i*-octane < cyclohexene < toluene (see Table 1). The fwhm in polar aprotic solvents, such as tetrahydrofuran, ethyl acetate, acetonitrile, and

TABLE 1: Lifetimes of 12′-Apo-β-caroten-12′-al in Various Solvents and Solvent Mixtures at 298 K

solvent	$R(n)$[a]	$R(\epsilon)$[a]	Δf[a]	λ_{max},[b] nm	fwhm[c] (cm^{-1})	λ_{pump}, nm	λ_{probe}, nm	τ_1,[d] ps	τ_3,[d] ps	A_1,[e] %	A_2,[e] %	br[f]	ref[g]
n-hexane	0.23	0.23	0	413	5010	390	390	224					18
						390	575	221					18
						390	630	217					18
						470	390	205					18
						430	860	200	2.5	−3	97	0.70	*h*
i-octane	0.24	0.24	0	413	5013	430	860	210	2.6	−3	97	0.73	*h*
cyclohexene	0.27	0.29	0.02	420	5274	430	860	192	2.9	−2	98	0.79	*h*
toluene	0.29	0.31	0.02	427	5126	430	860	201	4.0	−8	92	0.69	*h*
ethyl acetate + *i*-octane	0.24	0.42	0.18	417	5263	430	860	205	3.8	−4	96	0.69	*h*
diisopropyl ether	0.22	0.48	0.26	416	5425	430	860	194	4.1	−6	94	0.61	*h*
ethyl acetate + *i*-octane	0.24	0.53	0.29	419	5956	430	860	187	3.3	−7	93	0.59	*h*
diethyl ether	0.22	0.52	0.30	416	5451	430	860	173	3.2	−2	98	0.68	*h*
ethyl acetate	0.23	0.66	0.43	421	5235	430	860	105	2.0	−6	94	0.53	*h*
tetrahydrofuran	0.25	0.69	0.44	425	5225	390	390	92					18
						390	575	95					18
						390	630	85					18
						470	390	96					18
						430	860	79	1.8	−6	94	0.50	*h*
n-butanol	0.24	0.85	0.61	429	5755	430	860	35	2.0	−13	87	0.73	*h*
acetone	0.22	0.87	0.65	423	5241	370	740	17.4	1.3	−5	95	0.62	*h*
						390	780	19.0	1.3	−7	93	0.64	
						430	860	17.8	1.2	−13	87	0.46	
						445	890	17.9	1.2	−35	65	0.38	
								17.5[i]	1.3[i]				
ethanol	0.22	0.89	0.67	426	5510	390	390	22.6					18
						390	575	22.2					18
						390	630	18.5					18
						470	390	18.6					18
						430	860	16.4	1.4	−27	73	0.63	*h*
acetonitrile	0.21	0.92	0.71	424	5267	430	860	8.3	0.7	−24	76	0.57	*h*
methanol	0.20	0.91	0.71	426	5755	390	390	8.0					18
						390	575	8.2					18
						390	630	7.9					18
						470	390	6.7					18
						370	740	6.6	0.5	−4	96	0.79	*h, j*
						400	800	6.6	0.8	−6	94	0.72	*h, j*
						430	860	6.5	0.9	−27	73	0.59	*h*
						480	390	6.7					*h*
						490	390	6.8					*h*
						500	390	6.3					*h*
						525	390	6.2					*h*
								7.0[k]	0.9[k]				*h*

[a] $\Delta f = R(\epsilon) - R(n)$, where $R(\epsilon) = (\epsilon - 1)/(\epsilon + 2)$ and $R(n) = (n^2 - 1)/(n^2 + 2)$ with the dielectric constant ϵ and the index of refraction n of the solvent.[29] [b] Maximum peak position of the $S_0 \rightarrow S_2$ absorption spectrum. [c] Full width at half-maximum of the $S_0 \rightarrow S_2$ absorption band. [d] τ_1, τ_2, and τ_3 are time constants for ICT $\rightarrow S_0$, S_2 depopulation, and $S_1 \rightarrow$ ICT, respectively, obtained from the kinetic modeling described in the text. τ_2 values are limited by the time resolution of our experimental setup ($\leq$ca. 120 fs) and therefore not included here. [e] A_1 and A_2 are relative emission/absorption coefficients of the ICT and S_2 states, respectively, obtained from the fit results. [f] Relative branching ratio (br) from S_2 states to ICT (all to ICT when br = 1) and to S_1 (all to S_1 when br = 0). [g] τ_1 values from ref 18 were obtained from a simpler three-state-model ($S_2 \rightarrow S_1$/ICT $\rightarrow S_0$). Error limits are ±10%. [h] This paper. [i] Global fit for the four preceding data sets. [j] Data were measured at parallel pump−probe polarization. They agree within error limits with those measured at the magic angle. [k] Global fit for 390- and 400-nm pump.

acetone, is similar to that in cyclohexene or toluene and interestingly is independent of solvent polarity. The fwhm in other polar aprotic solvents (diethyl ether, chloroform, and dichloromethane) is larger and becomes even broader in polar protic solvents (methanol, ethanol, and *n*-butanol). This is shown in Figure 2D, where we compare absorption spectra of 12′-apo-β-caroten-12′-al in cyclohexene, acetonitrile, and methanol. The spectra in cyclohexene and in acetonitrile are very similar; however, the absorption band in methanol is more extended to longer wavelengths compared to that in acetonitrile, which has similar polarity. This effect is also seen for 8′-apo-β-caroten-8′-al in Figure 3.

The absorption maxima of 12′-apo-β-caroten-12′-al and 8′-apo-β-caroten-8′-al are summarized in Tables 1 and 2, respectively. Again, these values, however, cannot be simply correlated in terms of solvent polarizability and polarity. For the C_{40} carotenoid β-carotene, where the vibronic band structure is obvious, we have shown that the absorption peak position near 450 nm is linearly dependent on solvent polarizability, with a ca. 30 times stronger dependence on solvent polarizability than polarity.[30] We have applied a similar band analysis for 12′-apo-β-caroten-12′-al as follows. First, we could analyze the absorption spectra in nonpolar solvents by a sum of Gaussian bands with the same width (ca. 1800 cm^{-1}). From this, the band origin (0−0 transition) was estimated for each spectrum in nonpolar solvents. It was found that the 0−1 band position behaved very similar to the location of the apparent peak maximum. Second, we considered only the four polar aprotic solvents tetrahydrofuran, ethyl acetate, acetonitrile, and acetone, which have a similar fwhm as cyclohexene or toluene. Keeping the same Gaussian bandwidth for each vibronic band (0−0 to 0−5 band) as in the nonpolar case (ca. 1800 cm^{-1}), we then simulated the absorption spectrum with a sum of Gaussian peak functions and estimated the position of the 0−0 transition for these four polar aprotic solvents. Then, we investigated the correlation of the absorption maximum (in reciprocal centime-

TABLE 2: Lifetimes of 8′-Apo-β-caroten-8′-al in Various Solvents at 298 K

solvent	$R(n)^a$	$R(\epsilon)^a$	Δf^a	λ_{max}, nm	λ_{pump}, nm	λ_{probe}, nm	τ_1, ps	τ_3, ps	A_1,[b] %	A_2,[b] %	br[c]	ref
i-octane	0.24	0.24	0	456	450	900	24.8	1.1	−0.2	99.8	0.69	*d*
toluene	0.29	0.31	0.02		510	480	25.1					15
3-methylpentane	0.23	0.23	0		490	555	26.4					16, 32
tetrahydrofuran	0.25	0.69	0.44	463	450	900	25.8	1.5	−1.1	98.9	0.60	*d*
dichloromethane	0.26	0.73	0.47		490	$S_1 \rightarrow S_N$	14.1					32
acetone	0.22	0.87	0.65	458	450	900	15.5	1.4	−0.8	99.2	0.81	*d*
ethanol	0.22	0.89	0.67	465	490	$S_1 \rightarrow S_N$	17.1					32
					445	890	14.9	1.0	−2.2	97.8	0.60	*d*
acetonitrile	0.21	0.92	0.71	458	490	550	8.4					16
					445	890	8.1	0.5	−2.0	98.0	0.75	*d*
methanol	0.20	0.91	0.71	463	445	890	7.6	0.5	−2.3	97.7	0.75	*d*

[a] $\Delta f = R(\epsilon) - R(n)$, where $R(\epsilon) = (\epsilon - 1)/(\epsilon + 2)$ and $R(n) = (n^2 - 1)/(n^2 + 2)$ with the dielectric constant ϵ and the index of refraction n of the solvent.[29] [b] Relative amplitudes for the contribution of the time constants τ_1 and τ_2, respectively, obtained from the fit results. [c] Due to the relatively weak stimulated emission signals, the uncertainty of the branching ratio is high. [d] This paper.

ters) with solvent polarizability and polarity using a bilinear function (see, for example, ref 31):

$$\tilde{\nu}(1^1B_u^+) = [\tilde{\nu}_0 + aR(n) + b\{R(\epsilon) - R(n)\}] \qquad (1)$$

where $\tilde{\nu}_0$ is the $1^1B_u^+$ energy in the gas-phase limit; the *a* and *b* terms are used to account for the effects of solvent polarizability and (di)polarity, respectively; and the function $R(\epsilon) = (\epsilon - 1)/(\epsilon + 2)$ (with ϵ being the dielectric constant of the solvent)[29] considers permanent and induced dipole contributions. The experimental data for 12′-apo-β-caroten-12′-al in the aforementioned four nonpolar and four polar aprotic solvents are then expressed as

$$\tilde{\nu}\,(1^1B_u^+) = [(25\,480 \pm 230) - (11\,650 \pm 900)R(n) - (1270 \pm 80)\{R(\epsilon) - R(n)\}] \qquad (2)$$

in reciprocal centimeters, with the linear regression coefficient 0.98. The ca. 10 times smaller value of the *b* term compared to the *a* term in eq 2 indicates that the spectral shifts are much more sensitive to the change of the solvent polarizability function $R(n)$. Considering that an *a*/*b* ratio of about 30 was determined in our previous analysis for C_{40} carotenoids,[30] the results for 12′-apo-β-caroten-12′-al indicate that the role of solvent polarity is still minor but becomes more pronounced in the spectral shifts. For a better characterization of the solvent-induced changes of the absorption peak maxima, experimental data over a wide range of $R(n)$ values are desirable.

Steady-State Fluorescence Spectra. Room-temperature steady-state fluorescence/excitation spectra of 12′-apo-β-caroten-12′-al are shown in Figure 4 for *n*-hexane (A) and methanol (B). Steady-state absorption spectra (1) are also shown for comparison. Excitation at the absorption maximum produces a fluorescence spectrum (3) that has its maximum around 700 nm (in *n*-hexane) or 750 nm (in methanol). This feature could be attributed to the S_1/ICT states. Fluorescence excitation spectra (2) monitored at 700 nm are also included in Figure 4 and are normalized to the same maximum amplitude as the corresponding absorption spectra. They are very similar in shape. This is consistent with the interpretation that the observed emission originates from the S_1/ICT states, which are populated after internal conversion from S_2. Note also that, in both solvents, spectrum 3 has a blue shoulder around 500 nm, which resembles the mirror image of the $S_0 \rightarrow S_2$ transition. Therefore this blue wing could be assigned to weak $S_2 \rightarrow S_0$ fluorescence. The red shift of the fluorescence spectrum of the S_1/ICT $\rightarrow S_0$ transition in the polar methanol is stronger than that in *n*-hexane. It is interesting to note that the solvent-induced spectral shift of the S_1/ICT fluorescence is larger than that observed in the $S_0 \rightarrow S_2$ absorption spectra. A similar effect was observed in steady-state absorption/fluorescence studies of peridinin by, for example, Bautista et al.[20] and Shima et al.[25] The latter group interpreted this observation on the basis of the different dipole moments of the S_1 and S_2 states.[25] Our fluorescence spectra are consistent with the interpretation that the charge-transfer character of the ICT state is responsible for the observation of solvent-induced spectral shifts of the fluorescence spectrum in the wavelength range 500−800 nm.

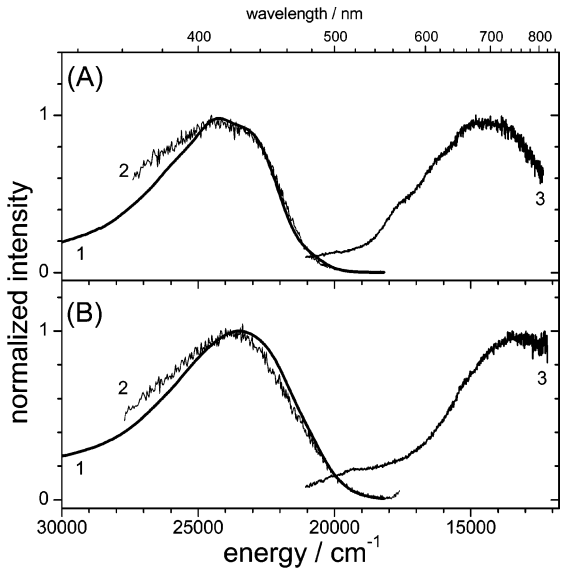

Figure 4. Steady-state absorption (1), fluorescence excitation (2), and fluorescence spectra (3) of 12′-apo-β-caroten-12′-al in (A) *n*-hexane and (B) methanol at room temperature. Fluorescence excitation spectra (2) were monitored at 700 nm. For fluorescence spectra, excitation wavelengths were 413 nm (3) for *n*-hexane and 425 nm (3) for methanol. The spectra were all normalized to their peak maxima.

Time-Resolved Transient Absorption/Stimulated Emission Signals and Their Kinetic Modeling. Typical signals for the intramolecular dynamics of 12′-apo-β-caroten-12′-al in different solvents at 298 K can be found in Figures 5 (acetonitrile) and 6 (*n*-hexane, ethyl acetate, and ethanol). The kinetics of the transient absorption/stimulated emission signals at 860 nm after excitation of 12′-apo-β-caroten-12′-al at 430 nm showed a strong dependence on the solvent environment. All experimental time traces in this work could be explained by using the kinetic model depicted in Figure 7 with a minimum number of adjustable parameters. It is a modified version of the scheme for peridinin in methanol proposed by van Grondelle and co-workers[26,27] on the basis of their time-resolved experiments in the visible region (see section 4).

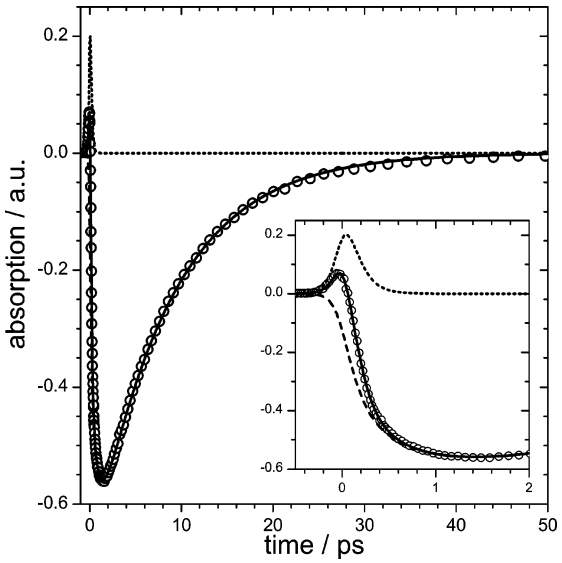

Figure 5. Example of a time-resolved transient absorption/stimulated emission signal for 12′-apo-β-caroten-12′-al in acetonitrile (○) at 298 K. $\lambda_{pump} = 430$ nm and $\lambda_{probe} = 860$ nm. The temporal evolution of the signal at early times is shown in the inset. The solid line represents the best fit obtained from the kinetic modeling described in the text. The different broken lines indicate contributions from $S_2 \rightarrow S_N$ absorption (···) and ICT $\rightarrow S_0$ emission (---) to the best fit.

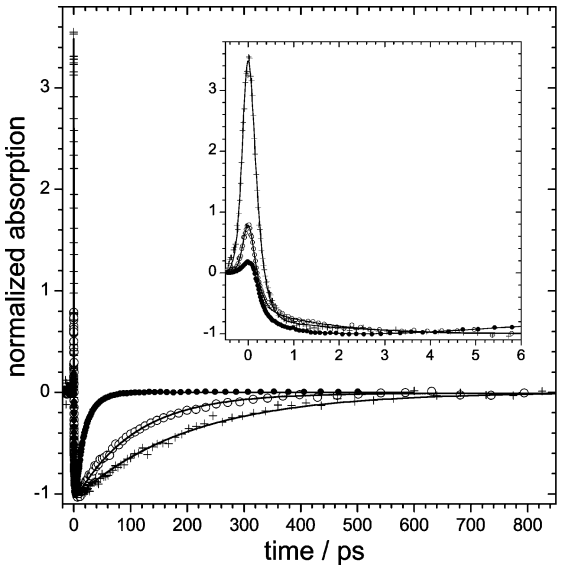

Figure 6. Examples of time-resolved transient absorption/stimulated emission signals from 12′-apo-β-caroten-12′-al measured in liquids of different polarity at 298 K: (●) in ethanol, (○) in ethyl acetate, and (+) in *n*-hexane. Signals are normalized to the maximum amplitude of the stimulated emission. $\lambda_{pump} = 430$ nm and $\lambda_{probe} = 860$ nm. The temporal evolution of the signals at early times is shown in the inset. Lines indicate the best fits from the kinetic modeling.

Within the mechanism presented in our paper, apocarotenals prepared in the S_2 state decay via two channels, leading to the S_1 and ICT states. The loss of S_2 population is evident from the decay of the strong $S_2 \rightarrow S_N$ absorption at very early times (Figures 5 and 6). The total S_2 depopulation rate constant is $k_2 = \tau_2^{-1}$, and the branching ratio (br) controls the flow of population of S_2 into either S_1 or ICT (e.g., br = 1 when all S_2 concentration is transferred to ICT). There is probably an equilibrium between the S_1 and ICT states. However, to model the data of the present study and previous experiments in ref 18, it is sufficient to include a relatively fast population transfer from S_1 to ICT ($k_3 = \tau_3^{-1}$, where τ_3 is in the picosecond regime).

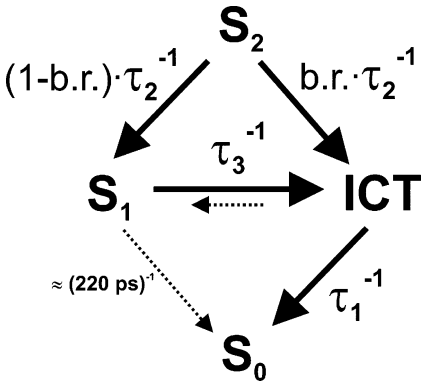

Figure 7. Kinetic scheme for the photoinduced excited-state dynamics of the apocarotenals. The processes symbolized by the solid arrows were needed for a successful fit of the experimental signals. The ICT $\rightarrow S_1$ backward reaction (shorter dashed arrow) in the S_1−ICT equilibrium was assumed to be much slower than the forward reaction. The fit results were insensitive to the $S_1 \rightarrow S_0$ step (longer dashed arrow), when its time constant was assumed to have the same value as in nonpolar solvents (e.g., ca. 220 ps for 12′-apo-β-caroten-12′-al).

This is responsible for the "round shape" of the stimulated emission at early times (Figure 5). The backward reaction (ICT $\rightarrow S_1$) is assumed to be slow enough that it does not affect the kinetics (dashed short horizontal arrow in the mechanism of Figure 7). Finally, the transition from the ICT state to the ground electronic state S_0 takes place with the rate constant $k_1 = \tau_1^{-1}$, as shown by the decay of the stimulated emission toward zero in Figures 5 and 6. We note that it was not necessary to include an "unrelaxed" ICT species in our work, different from the study of Papagiannakis et al.[27] (see section 4 for details). Furthermore, including a reasonable value of the time constant $\tau(S_1 \rightarrow S_0)$ for the decay of population from S_1 to S_0 (long dashed arrow in Figure 7) did not influence the fits due to the dominant population flux via the $S_1 \rightarrow$ ICT channel. The value for the $S_1 \rightarrow S_0$ time constant was assumed to be similar to that determined in nonpolar solvents (i.e., ca. 220 ps for 12′-apo-β-caroten-12′-al and ca. 25 ps for 8′-apo-β-caroten-8′-al, see section 4). Support for this assumption comes from previous ultrafast experiments for carotenoids without C=O substituents attached to the conjugated system, which possess only an S_1 state and exhibit no dependence of the $S_1 \rightarrow S_0$ IC time constant on solvent polarity.[2,17]

Figure 5 illustrates typical simulation results. All absorption−time profiles in this work were well-reproduced by the kinetic model with a typical regression coefficient of 0.9998. A Levenberg−Marquardt least-squares fitting procedure was used to extract the best-fit parameters for the time constants τ_1, τ_2, and τ_3, the branching ratio, and the absorption coefficients for ICT and S_2. In the final simulated signals (solid lines in Figures 5 and 6), the limited time resolution of our setup was also accounted for. The dashed line in the inset of Figure 5 illustrates the individual contribution of the ICT state to the total signal as obtained from the fitting procedure, and the dotted line is the corresponding absorption contribution from the initially formed S_2 state.

In addition, we performed modeling of our earlier data, specifically in the S_1/ICT $\rightarrow S_N$ excited-state absorption band, which was previously analyzed in the framework of a simpler consecutive model ($S_2 \rightarrow S_1$/ICT $\rightarrow S_0$).[18] Note that transient spectra recorded by van Grondelle and co-workers[27] for peridinin in nonpolar and polar solvents suggest that the ESA band observed in this spectral region consists of a mixture of S_1 and ICT contributions. In methanol and ethanol, where we have the most detailed data, very similar τ_3 (and also τ_1) values are

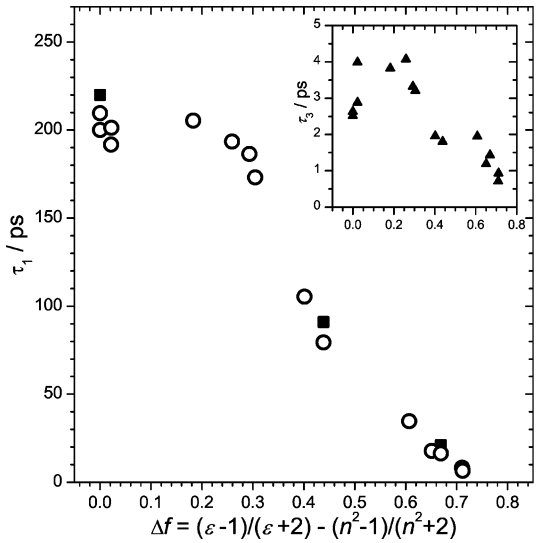

Figure 8. ICT → S_0 internal conversion time constants τ_1 of 12′-apo-β-caroten-12′-al in various solvents as a function of the solvent polarity function Δf at 298 K (see Table 1). (■) Transient absorption experiments in *n*-hexane, tetrahydrofuran, ethanol, and methanol in increasing order of solvent polarity.[18] (○) Values extracted from the decay of the transient stimulated emission in the near IR (this work). Inset: Time constants τ_3 for S_1 → ICT shown as a function of Δf. See also Table 1.

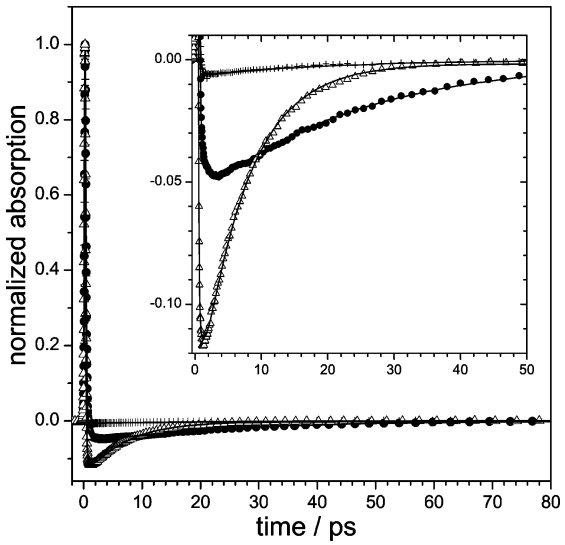

Figure 9. Time-resolved transient absorption/stimulated emission signals from 8′-apo-β-caroten-8′-al measured in liquids of different polarity at 298 K: (+) in *i*-octane, (●) in tetrahydrofuran, and (△) in methanol. Signals are normalized to the absorption maximum of the S_2 → S_N peak. λ_{pump} = 445 (methanol) and 450 nm (*i*-octane, tetrahydrofuran); λ_{probe} = 890 nm (methanol) and 900 nm (*i*-octane, tetrahydrofuran). Temporal evolution of the signals at early times is shown in the inset. Lines indicate the best fits from the kinetic modeling.

obtained from the fitting results in the ESA and stimulated emission bands. This is consistent with the assignment of this process to ICT formation from S_1 (visible in these transient profiles as a "round" shape of the rise of the excited-state absorption). The extracted time constant τ_2 was typically within the time resolution of our experimental setup. Therefore we can estimate only an upper limit for the depopulation of the S_2 state. The resulting fit parameters are summarized in Tables 1 and 2.

We carried out a sensitivity analysis for the fit parameters (time constants τ_1, τ_2, and τ_3; absorption coefficients of the S_2 and ICT species; and the branching ratio br). Complex shapes of the transient absorption/stimulated emission kinetics were observed only in the first few picoseconds, and therefore the considerably larger τ_1 value for the final ICT decay on longer time scales was always well-determined: for example, practically identical τ_1 values were found when τ_3 or the branching ratio br were intentionally varied by ±10% from the best fit. When τ_1, br, or the absorption coefficient of the ICT state was changed by ±10% from the best fit and fixed, it was not possible to reach a good fit quality (also in the curved region of the signal near 0.5−1.5 ps; see, for example, Figure 5), indicating that those values were well and independently determined. Similarly, the fit quality deteriorated significantly when τ_3 was deliberately changed by ±10% and could not be improved by varying other parameters like the absorption coefficient of the S_2 → S_N transition, showing again that τ_3 is reliably determined. As a result, all fits converged to a well-defined global minimum of χ^2.

Our model does not rule out the presence of a back-reaction ICT → S_1. On the contrary, our results are fully consistent with such a process. On the basis of parameter sensitivity studies, we can estimate the influence of such a back-reaction: Taking our methanol signal at λ_{probe} = 860 nm as an example, we still get an acceptable fit to our near-IR signals when we include a back-reaction with a time constant of 10 ps. The other parameters then change only slightly: τ_1 = 5.8 ps (slightly smaller than the value in Table 1 to compensate the additional population loss due to back-reaction from ICT to S_1), τ_3 = 1.1 ps (compared to 0.9 ps without back-reaction), and a branching ratio of 0.57 (before, 0.59). Note that the three parameters τ_1, τ_3, and branching ratio are completely insensitive to the change of the time constant of the back-reaction for values >15 ps in the case of methanol. Similarly, in *n*-hexane (with a much larger τ_1 value), τ_1, τ_3, and the branching ratio can be independently determined regardless of the time constant of the back-reaction for values >15 ps.

Solvent and Probe Wavelength Dependence of τ_1 and τ_3. Solvent-dependent fitting results for 12′-apo-β-caroten-12′-al are summarized in Figure 8 and Table 1. Solvent polarity has characteristic influences on the relative amplitude ratio and the lifetime (τ_1) of the stimulated emission in the near-IR region. First, the amplitude ratio of stimulated emission (ICT → S_0) to absorption (S_2 → S_N) increased with increasing polarity of the solvent. Second, the τ_1 values were strongly dependent on solvent polarity. τ_1 was almost linearly correlated with polarity from medium solvent polarity onward (Δf > 0.4), where Δf is expressed by the difference of the permanent and induced dipole moment function $R(\epsilon)$ and the electronic polarization function $R(n)$. Figure 6 contains three time traces measured in *n*-hexane, ethyl acetate, and ethanol, clearly illustrating the faster decay kinetics in more polar solvents. Third, there seems to be an onset of such solvent dependence of the τ_1 values. Figure 8 illustrates this clearly. For instance, in the lower polarity range (Δf = 0−0.3), the τ_1 values were not so sensitive to the solvent polarity, and therefore they could not be linearly correlated with the solvent polarity any longer. τ_1 appears to level off as Δf approaches 0. Interestingly, this effect is also seen in the solvent polarity dependence of the τ_1 values of 8′-apo-β-caroten-8′-al; however, the onset of such solvent-polarity dependence on τ_1 appears at a higher Δf value compared to the 12′-species: τ_1 values in *i*-octane (Δf = 0) and tetrahydrofuran (Δf = 0.44) were practically the same but decreased significantly in more polar solvents such as acetone, ethanol, acetonitrile and methanol (see Table 2). Therefore, it is important to collect extensive experimental data for different apocarotenals over a wide range of solvent polarity because the onset of polarity-dependent

TABLE 3: Temperature Dependence of τ_1 of 12′-Apo-β-caroten-12′-al in Various Solvents

									E_a (ICT → S_0), kJ mol^{-1}	
solvent	T, K	$\epsilon(T)$[a]	$n(T)$[a]	$\Delta f(T)$[a]	τ_1^{exp}, ps	$\tau_1^{corr}(T)$,[b] ps	τ_3^{exp}, ps	br	exp	corr
ethanol	283	26.6	1.365	0.672	18.4	20.0	1.15	0.64	7.7 ± 0.3	12.8 ± 0.5
	293	25.2	1.361	0.669	16.3	16.8	1.09	0.65		
	303	23.8	1.357	0.665	15.2	14.8	1.02	0.65		
	313	22.4	1.353	0.660	13.6	12.3	1.14	0.70		
	323	21.0	1.349	0.655	12.4	10.5	1.04	0.69		
	333	19.6	1.35	0.649	11.2	8.7	1.04	0.67		
methanol[c]	288	34.6	1.330	0.714	6.7	7.5	0.90	0.62	5.2 ± 0.2	14.5 ± 0.4
	293	33.7	1.329	0.713	6.5	6.9	0.84	0.64		
	298	32.8	1.326	0.712	6.2	6.2	0.95	0.66		
	303	31.9	1.325	0.710	6.1	5.7	0.90	0.65		
	308	31.0	1.323	0.709	5.8	5.2	0.85	0.65		
	318	29.2	1.319	0.706	5.4	4.2	0.81	0.64		
acetonitrile	283	38.6	1.349	0.712	8.3	8.5	0.77	0.62	1.7 ± 0.3	4.4 ± 0.6
	293	37.1	1.344	0.711	8.2	8.3	0.78	0.67		
	303	35.6	1.339	0.711	8.0	7.9	0.70	0.69		
	313	34.1	1.335	0.710	7.8	7.5	0.60	0.70		
	323	32.6	1.330	0.709	7.8	7.1	0.64	0.81		
	333	31.1	1.325	0.708	7.3	6.3	0.57	0.82		
ethyl acetate	283	6.3	1.378	0.409	92.1	94.7	2.69	0.53	2.6 ± 0.7	4.2 ± 0.8
	293	6.1	1.373	0.403	95.3	96.2	2.43	0.57		
	303	5.9	1.367	0.396	93.5	92.6	2.35	0.62		
	313	5.7	1.362	0.389	85.0	82.4	2.29	0.62		
	323	5.5	1.357	0.382	81.0	76.9	2.00	0.67		
	333	5.3	1.352	0.374	82.0	76.1	1.35	0.68		

[a] Data taken from refs 34 and 35. $\Delta f = (\epsilon - 1)/(\epsilon + 2) - (n^2 - 1)/(n^2 + 2)$ with the dielectric constant ϵ and the index of refraction n of the solvent. [b] τ_1 values corrected for the temperature-induced solvent polarity change. [c] Data were measured at parallel pump−probe polarization. However, in methanol they agree within error limits with those measured at the magic angle.

intramolecular dynamics seems to be characteristic for the molecular system.

Surprisingly, ICT → S_0 stimulated emission was observed even in nonpolar solvents such as *n*-hexane, *i*-octane, cyclohexene, and toluene. It was weak, but still clearly detectable, as can be seen, for example, from the data for 12′-apo-β-caroten-12′-al in *n*-hexane in Figure 6, and this is one of the central results of the present paper. To our knowledge, there have been no previous reports of stimulated emission for carbonyl carotenoids in nonpolar solvents. For instance, stimulated emission was not detected in the case of peridinin dissolved in *n*-hexane (despite the detection of steady-state fluorescence in this wavelength region),[21,25] leading to the conclusion that the stimulated emission band and a superimposed broad excited-state absorption band might be counterbalanced.[21,22]

Results of kinetic modeling for stimulated emission from 8′-apo-β-caroten-8′-al at 890 and 900 nm are summarized in Table 2 for various solvents. Figure 9 compares three representative curves in *i*-octane, tetrahydrofuran, and methanol. Although several ultrafast time-resolved pump−probe experiments have been reported for 8′-apo-β-caroten-8′-al,[15,16,32] such a stimulated emission in the near-IR region has not been observed previously. The amplitude of the stimulated emission in a given solvent was much weaker than that of the S_2 → S_N absorption (and also weaker than that of the stimulated emission of 12′-apo-β-caroten-12′-al in the same solvent in this wavelength range). This is also clear from Figure 9, where we normalized the experimental data in several solvents to the absorption maxima of the S_2 → S_N transition (for parameters, see Table 2). Again, the intensity ratio of stimulated emission and S_2 → S_N absorption increased with solvent polarity. A quantitative evaluation of the S_2 → S_N absorption/ICT → S_0 emission amplitude ratio for each apocarotenal and a full comparison of the absolute amplitudes of the stimulated emission bands for the 12′- and 8′-species will require measurements of time-resolved spectral profiles over a wider wavelength range.

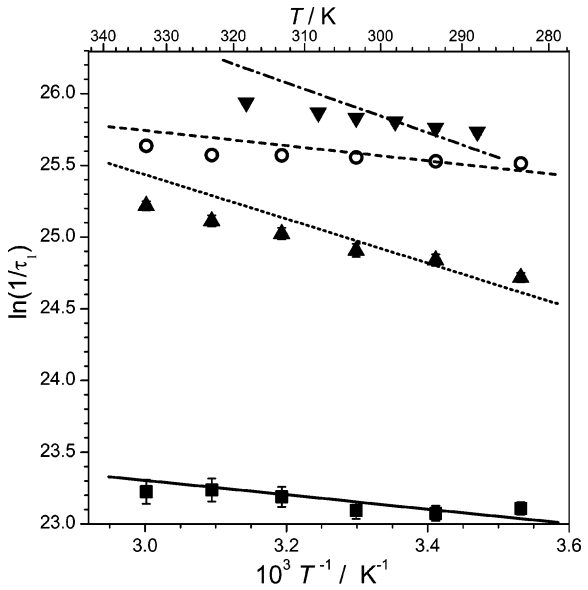

Figure 10. Arrhenius plot of the internal conversion time constants τ_1 from stimulated emission signals of 12′-apo-β-caroten-12′-al in ethyl acetate (■), acetonitrile (○), ethanol (▲), and methanol (▼). λ_{pump} = 430 nm and λ_{probe} = 860 nm. Experimental values of τ_1 are plotted as symbols with error bars. Lines are values without the contribution of the temperature-dependent polarity change (see text): evaluation for (—) ethyl acetate, (···) ethanol, (---) acetonitrile, and (— · —) methanol.

The time constant τ_3 was required to completely fit the kinetic data for 12′-apo-β-caroten-12′-al (0.5−4.1 ps) and 8′-apo-β-caroten-18′-al (0.5−1.5 ps). There was no such clear correlation of the τ_3 values with solvent polarity, as seen in the case of τ_1. On average τ_3 appears to be larger in nonpolar solvents and smaller in polar solvents, indicating an acceleration of the ICT → S_1 transition in polar solvents.

Pump Wavelength Dependence of τ_1. The excitation wavelength dependence of the τ_1 values of 12′-apo-β-caroten-

12′-al was investigated in two different solvents: acetone (polar aprotic) and methanol (polar protic). For acetone we obtained data at four different excitation wavelengths (370, 390, 430, and 445 nm), which prepared 12′-apo-β-caroten-12′-al molecules with different amounts of excess energy in S_2 (see also the steady-state absorption spectrum in acetone in Figure 2B). In this range, τ_1 values obtained from stimulated emission signals were found to be insensitive to the excitation wavelength: τ_1 = 17.4, 19.0, 17.8, and 17.9 ps after excitation at 370, 390, 430, and 445 nm, respectively (corresponding probe wavelengths were 740, 780, 860, and 890 nm). These results are also summarized in Table 1. In the case of methanol, measurements were performed at seven different excitation wavelengths in the range 370−525 nm, which cover the whole $S_0 \rightarrow S_2$ band (Figure 2D); for corresponding probe wavelengths and time constants, see Table 1. These measurements yielded very similar τ_1 values between 6.8 and 6.2 ps, where the two smallest values were observed on the far red edge of the band.

Temperature Dependence of τ_1. We also investigated the temperature dependence of τ_1 for 12′-apo-β-caroten-12′-al over the temperature range 283−333 K. Experimental τ_1 values measured in four different solvents are presented in an Arrhenius plot in Figure 10 and summarized in Table 3. In all solvents, the ICT $\rightarrow S_0$ internal conversion process became faster at higher temperatures. The degree of temperature dependence of the τ_1 values was solvent-dependent, which was reflected in the values of the apparent experimental activation energies (E_a). They increase in the order acetonitrile (1.7 kJ mol^{-1}) $\approx$ ethyl acetate (2.6 kJ mol^{-1}) < methanol (5.2 kJ mol^{-1}) < ethanol (7.7 kJ mol^{-1}). First of all, it should be noted that such small apparent activation energies on the order of a few times RT are characteristic for thermally activated internal conversion processes (see, for example, ref 33). However, a more detailed separation of at least two effects is necessary at this point.

First, the solvents become "less polar" (i.e., they have a smaller Δf) at higher temperature and therefore larger τ_1 values would be expected if the temperature dependence of the τ_1 values is entirely due to the polarity change.[34,35] However, apparently, our experimental τ_1 values became smaller at higher temperatures. This indicates that there must be another counteracting temperature dependence that surpasses the polarity effect. In the following, we try to separate the two contributions. The refractive index (n) and the dielectric constant (ϵ) have a negative temperature dependence. On the basis of the evaluation in refs 34 and 35, the temperature dependence of n and ϵ over the temperature range 280−340 K (T in Kelvin) can be expressed as

$$n(T) = 1.383 - (5.117 \times 10^{-4})T \text{ and } \epsilon(T) = 11.9 - 0.02T \text{ for ethyl acetate} \quad (3)$$

$$n(T) = 1.353 - (4.696 \times 10^{-4})T \text{ and } \epsilon(T) = 81.4 - 0.15T \text{ for acetonitrile} \quad (4)$$

$$n(T) = 1.369 - (4.000 \times 10^{-4})T \text{ and } \epsilon(T) = 66.5 - 0.14T \text{ for ethanol} \quad (5)$$

$$n(T) = 1.336 - (3.854 \times 10^{-4})T \text{ and } \epsilon(T) = 86.6 - 0.18T \text{ for methanol} \quad (6)$$

These values and the resulting temperature-dependent $\Delta f(T)$ are listed in Table 3. The temperature dependence of the τ_1 values can then be approximated as

$$\tau_1^{\text{corr}}(T) \approx \tau_1^{\text{exp}}(T, \Delta f)\left[\frac{\Delta f_0 - \Delta f^{298\text{K}}}{\Delta f_0 - \Delta f(T)}\right] \quad (7)$$

where $\tau_1^{\text{corr}}(T)$ is the temperature-dependent τ_1 value without considering the influence of the temperature-dependent solvent polarity, $\tau_1^{\text{exp}}(T, \Delta f)$ is the measured experimental τ_1 value, Δf_0 is the Δf axis intercept for $\tau_1 \rightarrow 0$ (see below), $\Delta f^{298\text{K}}$ is the Δf value at 298 K for a particular solvent, and $\Delta f(T)$ are the temperature-dependent Δf values based on eqs 3−6. Given our measured polarity dependence of τ_1 values in different solvents at 298 K and assuming linearity over the Δf range 0.40−0.72, $\Delta f_0 = 0.73$ was estimated at 298 K when τ_1 approaches zero. It is likely that Δf_0 is a temperature-independent quantity, because the temperature dependence of n is rather small and $R(\epsilon)$ will always approach unity for large ϵ. We note that this simple correction is valid if the τ_1 versus Δf curves at different temperatures yield also an approximately linear relationship.

The resulting Arrhenius plots without the contribution due to the temperature-induced polarity change are shown in Figure 10 as lines. First of all, as expected, the temperature dependence is now stronger, and the correction is largest in methanol. The order of activation energies is then given as ethyl acetate (4.2 kJ mol^{-1}) $\approx$ acetonitrile (4.4 kJ mol^{-1}) < ethanol (12.8 kJ mol^{-1}) $\approx$ methanol (14.5 kJ mol^{-1}). Again, even after this correction, the activation energies for the IC step ICT $\rightarrow S_0$ (τ_1) in the temperature range 288−333 K are still on the order of a few times RT. Such small values are typical for internal conversion and other nonradiative processes, where rate constants slightly increase with the excess energy in the initial state. It is interesting to note that the activation energies of ethyl acetate and acetonitrile are similar but those of the two alcohols are ca. 3 times larger. The reason for this is not yet understood. Such variations have been also observed for other thermally activated IC processes in liquids.[33]

4. Discussion

Solvent Dependence of τ_1. As the central finding of this paper, we have identified stimulated emission in the near-IR region of two carbonyl carotenoids even in nonpolar solvents. This points out that a state with intramolecular charge-transfer character is populated already in nonpolar media. Interestingly, so far experimental evidence for such an ICT state in the excited-state dynamics of peridinin[21,22] or *all-trans*-retinal[36] has been reported only in polar solvents, whereas, for example, peridinin in nonpolar solvents exhibited two weak excited-state absorption features in the near-IR region.

The present study considerably extends our knowledge of the polarity dependence of the ICT $\rightarrow S_0$ transition of apocarotenals, especially for 12′-apo-β-caroten-12′-al, due to the large number of newly studied solvents, which cover a wide range of polarities. For $\Delta f > 0.4$, an almost linear dependence of τ_1 on Δf is found, whereas τ_1 appears to level off toward lower Δf, extrapolating to a value of around 220 ps for $\Delta f \rightarrow 0$. This behavior is comparable to that reported for peridinin, where at high polarities τ_1 values are very similar to those of 12′-apo-β-caroten-12′-al, and a leveling-off is observed at low Δf, approaching a smaller value of 160 ps.[23] For 8′-apo-β-caroten-8′-al the conjugated system is more extended, and a relatively fast internal conversion is already observed in alkanes (ca. 25 ps). This faster nonradiative decay is expected due to the decreasing energy gap between the ground and the first excited state when the conjugation length of the polyene system increases.[37] Still a pronounced decrease of τ_1 is found, reaching

a value of 7.6 ps in methanol, indicating the presence of the ICT state. We have shown in this paper that the onset of such a leveling-off behavior in the solvent polarity dependence of the time constant τ_1 obviously depends on the length of the conjugated system ($\Delta f \approx 0.3$ and 0.6 for the 12′- and 8′-species, respectively).

Photoinduced Dynamics of Apocarotenals upon Excitation to S_2 and Their Implications for the Excited-State Processes of Peridinin and Other Carbonyl Carotenoids. van Grondelle and co-workers[26,27] carried out ultrafast experiments for peridinin in methanol in the visible region using two- and three-pulse techniques. They were modeled using global and target analysis methodologies. The key features of their model are as follows: After photoexcitation to S_2, an ultrafast internal conversion takes place (ca. 100 fs), which populates both the S_1 and an "unrelaxed" ICT state. The latter subsequently decays to a "relaxed" ICT state with a time constant of 2.6 ps after 400 nm excitation (the reported value for the relaxation process upon 530 nm excitation is 1.2 ps). The ICT state is preferentially populated with a branching ratio of about 95% in methanol. They postulate that S_1 and ICT exist as closely coupled entities connected by a relatively fast equilibrium, with an equilibration time constant of about 5 ps.

Our kinetic modeling, which involves an equilibrium (with a fast forward and a slow backward reaction) between the S_1 and ICT states as its central feature, is similar to their approach. However, there are also important differences between our kinetic scheme and the model by Papagiannakis et al.[26,27] and earlier suggestions by Zigmantas et al.[21,22] First of all, our kinetic model does not include the formation of an "unrelaxed" ICT state to explain the additional picosecond component observed in the near-IR traces. To explain this type of feature, Zigmantas et al. introduced an additional kinetic component in their fitting procedure for peridinin, where the sign of its amplitude is opposite to the sign of the amplitude of the final ICT $\rightarrow S_0$ transition. While this is a mathematically feasible description of the experimental profiles, it is not compatible with the underlying kinetics, because it would imply the formation of a species that generates an absorption feature emerging on a picosecond time scale, which is superimposed on the ICT stimulated emission. Instead, if an unrelaxed and a relaxed ICT species would be formed consecutively, the shape of the SE profile should be due to the superposition of two negative-going spectral features of two emitting ICT species having amplitudes with the same sign.

Here we offer a simpler explanation for the additional picosecond component in the stimulated emission traces in the near IR, which can also explain the identical time constants observed, for example, in our S_1/ICT $\rightarrow S_N$ absorption profiles.[18] The observed kinetics can be due to the delayed formation of some fraction of ICT population from S_1 via the S_1-ICT equilibrium and produce the "round shape" in the ICT $\rightarrow S_0$ and S_1/ICT $\rightarrow S_N$ profiles at early times. Also, such an explanation could possibly resolve the remaining discrepancies mentioned in the modeling of van Grondelle and co-workers, who included an unrelaxed peridinin ICT species that was, however, "not devoid of S_1 absorption features" and had an "unrealistic 2.6 ps lifetime."[27] These dynamics could be simply due to S_1-ICT equilibration. A further piece of support for our mechanism comes from the presence of a picosecond component τ_3 in the stimulated emission signals even in nonpolar solvents, which is similar to the one observed in polar solvents. This rules out the explanation that the observed dynamics might be due to a solvent relaxation process around the ICT state, that is, reorientation of the solvent dipoles around the solute, proposed as one possible interpretation for the similar dynamics of peridinin in polar solvents.[27] Such a mechanism is not supported in nonpolar solvents, yet we observe similar dynamics giving support to the interpretation that it is rather an intramolecular process of the carotenoid, like the transition from S_1 to ICT suggested here, which is affecting the observed kinetics.

With respect to earlier and our present work, another puzzling detail must be mentioned. So far no stimulated emission in the near IR has been reported for peridinin in nonpolar solvents like *n*-hexane, although appreciable fluorescence was observed in the wavelength range between 600 and (at least) 850 nm. Zigmantas et al.[20,21] proposed that a broad excited-state absorption (ESA) band is present in this region, which cancels the stimulated emission resulting in an almost flat spectrum in the near-IR range, with the exception of two weak absorption features, which were assigned to ESA from the S_1 state. For peridinin in methanol, the fluorescence spectrum is extending further into the IR and stimulated emission is detected in time-resolved measurements.[21] Our steady-state fluorescence spectra for 12′-apo-β-caroten-12′-al in *n*-hexane and methanol show behavior similar to that of peridinin, with the near-IR emission in methanol having a larger red shift than in *n*-hexane (Figure 4). It is possible that a reduction of the ICT$-S_0$ energy gap together with an increase of the ICT$-S_N$ energy gap in the near IR produces a red shift of stimulated emission and a blue shift of the excited-state absorption, and therefore a better separation of the bands, such that stimulated emission can be detected. Obviously, in the apocarotenal systems investigated in our present study, the energetic positions of the states involved are more favorable, so that stimulated emission can be already detected in nonpolar solvents.

Additional time-resolved experiments will be certainly helpful to refine the kinetic mechanism of Figure 7. For instance, one could introduce an additional dump pulse in a pump−probe experiment, to deplete the ICT population. Such a type of measurement, as for instance demonstrated by van Grondelle and co-workers for peridinin in methanol,[26,27] could answer such questions as, for example, how quickly the S_1-ICT equilibrium is reestablished and whether short-lived ground-state intermediates are present in S_0.

Influence of Pump and Probe Wavelengths on τ_1. In this work, the dependence of τ_1 on excitation wavelength was investigated for 12′-apo-β-caroten-12′-al in acetone and methanol. In both cases the τ_1 values obtained from the stimulated emission decays were almost independent of λ_{pump} over the wavelength range 370−445 nm. For methanol, we have carried out additional experiments using another setup[18] where 12′-apo-β-caroten-12′-al was excited further on the red edge of the $S_0 \rightarrow S_2$ band at the wavelengths 480−525 nm and probed at 390 nm. Again τ_1 values were essentially constant, with only a very small acceleration by about 0.5 ps at the two highest wavelengths. Our results can be compared with an earlier study from Zigmantas et al.,[22] in which the pump wavelength dependence of τ_1 was characterized for peridinin in *n*-hexane (nonpolar), acetonitrile (polar aprotic), and methanol and ethylene glycol (polar protic). In the wavelength range from the blue edge to the maximum of the $S_0 \rightarrow S_2$ absorption spectrum (475 nm in the case of peridinin), τ_1 was independent of the pump wavelength, as determined from their time-resolved profiles in the near IR recorded at 950 nm [1700 nm ($S_1 \rightarrow S_2$) for *n*-hexane]. This is in good agreement with our results for 12′-apo-β-caroten-12′-al. For peridinin in *n*-hexane and acetonitrile, this behavior persisted to even larger pump wavelengths located

on the far red side of the $S_0 \rightarrow S_2$ absorption spectrum, whereas for the polar protic solvents a pronounced reduction of τ_1 up to about a factor of 2 was observed. To interpret these results, Zigmantas et al. assumed the formation of two different forms of peridinin in polar protic solvents, where a "red"-absorbing ground-state species is produced by hydrogen bonding via the carbonyl group. This species was thought to be responsible for the reduction of τ_1, pointing toward another factor (apart from the solvent polarity) that influences the dynamics of this IC step.

Interestingly, our results for 12′-apo-β-caroten-12′-al in methanol do not show such a strong dependence in methanol, with less than 10% decrease of τ_1 at the highest pump wavelength. Still an unusual asymmetric broadening of the $S_0 \rightarrow S_2$ absorption band toward longer wavelengths is observed in methanol and other polar protic solvents but not in polar aprotic ones (see, for example, Figure 2D). If different "red"-absorbing ground-state species exist, as postulated for peridinin in methanol,[22] their relaxation behavior appears to be similar in the case of 12′-apo-β-caroten-12′-al.

As far as the probe wavelength dependence of τ_1 is concerned, we observed only a mild reduction of τ_1 with increasing λ_{probe}.[18] The values obtained from the present experiments employing near-IR probe wavelengths are still within the error limits of both studies. This indicates that all τ_1 values determined from the $S_0 \rightarrow S_2$, S_1/ICT $\rightarrow S_N$, and ICT $\rightarrow S_0$ bands were not particularly sensitive to the probe wavelength for these types of solvents. From this, it seems that the S_1 and ICT states exist as closely coupled states.

5. Conclusions

We have investigated the excited-state dynamics of the aldehyde-substituted carotenoids 12′-apo-β-caroten-12′-al and 8′-apo-β-caroten-8′-al by recording their transient absorption/stimulated emission response in the near-IR region. A strong ultrafast initial spike is due to $S_2 \rightarrow S_N$ absorption, which is followed by formation of stimulated emission. Interestingly, stimulated emission was observed in all solvents: strong in polar media and weaker in nonpolar ones. This indicates the involvement of a state with intramolecular charge transfer (ICT) character in the excited-state dynamics, regardless of solvent polarity. The experimental results have been analyzed on the basis of a kinetic model, which features ultrafast excited-state branching from S_2 to the S_1 and ICT states, where only the latter exhibits stimulated emission. A delayed formation of a part of the stimulated emission is assigned to the $S_1 \rightarrow$ ICT transition ($\tau_3 = 0.5-4.1$ ps, depending on the solvent). Because it is also present in nonpolar solvents, this component cannot be due to solvent relaxation around the ICT state.

The lifetime τ_1 for the ICT $\rightarrow S_0$ step was strongly dependent on solvent polarity, and this behavior has been fully characterized by measurements in 13 solvents and two solvent mixtures, covering a wide range of solvent polarities. Good agreement has been found with our previous measurements of τ_1 for 12′-apo-β-caroten-12′-al in *n*-hexane, tetrahydrofuran, ethanol, and methanol, which probed the dynamics by recording the recovery of the ground-state bleach ($S_0 \rightarrow S_2$) and the excited-state absorption (S_1/ICT $\rightarrow S_N$).[18] All τ_1 values determined from the $S_0 \rightarrow S_2$, S_1/ICT $\rightarrow S_N$, and ICT $\rightarrow S_0$ bands are therefore similar in all solvents. No dependence of τ_1 on excitation wavelength has been found, particularly in methanol, where only after excitation on the far red side of the $S_0 \rightarrow S_2$ band was a minor reduction by 10% observed. This is in contrast to peridinin in methanol, where reduction by a factor of 2 was found and ascribed to the presence of additional "red"-absorbing ground-state species.[22] If these are present in the case of 12′-apo-β-caroten-12′-al, they obviously show only slightly different relaxation behavior. The temperature dependence of the time constant τ_1 for the ICT $\rightarrow S_0$ transition of 12′-apo-β-caroten-12′-al in different solvents was well described by Arrhenius-type behavior with small apparent activation energies of a few times *RT*, which are typical for radiationless processes.

The kinetic model used in the present work is the simplest one to account for the experimental observations obtained so far in the apocarotenal systems. A direct $S_1 \rightarrow S_0$ internal conversion step (e.g., in the case of 12′-apo-β-caroten-12′-al with a fixed time constant of $\tau_1 \approx 220$ ps, typical for nonpolar solvents) and an ICT $\rightarrow S_1$ back-reaction (with a time constant >15 ps) could have been included in our modeling. The kinetic modeling results based on the available experimental data would have been, however, not affected by such steps. In polar solvents, the main flux of population will in any case occur via the $S_2 \rightarrow$ ICT $\rightarrow S_0$ and $S_2 \rightarrow S_1 \rightarrow$ ICT $\rightarrow S_0$ routes.

Acknowledgment. Financial support from the Alexander von Humboldt foundation in the framework of the Sofja Kovalevskaja program and the German Science Foundation is gratefully acknowledged. We are indebted to J. Schroeder and D. Schwarzer for helpful discussions and experimental advice. We are also thankful to J. Troe, K. Luther, V. G. Ushakov, and J. Gierschner. Generous experimental support from R. Bürsing and D. A. Wild is gratefully acknowledged. Fluorescence data were provided by J. Seehusen. We also thank the BASF AG, and here especially H. Ernst, for providing the highly purified *all-trans*-apocarotenal samples and extensive advice.

References and Notes

(1) Frank, H. A.; Young, A. J.; Britton, G.; Cogdell, R. J. *The Photochemistry of Carotenoids*, 1st ed.; Kluwer: Dordrecht, The Netherlands, 1999; Vol. 8.
(2) Polívka, T.; Sundström, V. *Chem. Rev.* **2004**, *104*, 2021.
(3) Tavan, P.; Schulten, K. *J. Chem. Phys.* **1986**, *85*, 6602.
(4) Tavan, P.; Schulten, K. *Phys. Rev. B* **1987**, *36*, 4337.
(5) Sashima, T.; Koyama, Y.; Yamada, T.; Hashimoto, H. *J. Phys. Chem. A* **2000**, *104*, 5011.
(6) Koyama, Y.; Rondonuwu, F. S.; Fujii, R.; Watanabe, Y. *Biopolymers* **2004**, *74*, 2.
(7) Cerullo, G.; Polli, D.; Lanzani, G.; De Silvestri, S.; Hashimoto, H.; Cogdell, R. J. *Science* **2002**, *298*, 2395.
(8) Gradinaru, C. C.; Kennis, J. T. M.; Papagiannakis, E.; van Stokkum, I. H. M.; Cogdell, R. J.; Fleming, G. R.; Niederman, R. A.; van Grondelle, R. *Proc. Natl. Acad. Sci. U.S.A.* **2001**, *98*, 2364.
(9) Wohlleben, W.; Buckup, T.; Herek, J. L.; Cogdell, R. J.; Motzkus, M. *Biophys. J.* **2003**, *85*, 442.
(10) Wohlleben, W.; Buckup, T.; Hashimoto, H.; Cogdell, R. J.; Herek, J. L.; Motzkus, M. *J. Phys. Chem. B* **2004**, *108*, 3320.
(11) Billsten, H. H.; Pan, J.; Sinha, S.; Pascher, T.; Sundström, V.; Polívka, T. *J. Phys. Chem. A* **2005**, *109*, 6852.
(12) Papagiannakis, E.; van Stokkum, I. H. M.; Vengris, M.; Cogdell, R. J.; van Grondelle, R.; Larsen, D. S. *J. Phys. Chem. B* **2006**, *110*, 5727.
(13) Larsen, D. S.; Papagiannakis, E.; van Stokkum, I. H. M.; Vengris, M.; Kennis, J. T. M.; van Grondelle, R. *Chem. Phys. Lett.* **2003**, *381*, 733.
(14) Christensen, R. L.; Barney, E. A.; Broene, R. D.; Galinato, M. G. I.; Frank, H. A. *Arch. Biochem. Biophys.* **2004**, *430*, 30.
(15) Wasielewski, M. R.; Kispert, L. D. *Chem. Phys. Lett.* **1986**, *128*, 238.
(16) He, Z.; Gosztola, D.; Deng, Y.; Gao, G.; Wasielewski, M. R.; Kispert, L. D. *J. Phys. Chem. B* **2000**, *104*, 6668.
(17) Kopczynski, M.; Lenzer, T.; Oum, K.; Seehusen, J.; Seidel, M. T.; Ushakov, V. G. *Phys. Chem. Chem. Phys.* **2005**, *7*, 2793.
(18) Wild, D. A.; Winkler, K.; Stalke, S.; Oum, K.; Lenzer, T. *Phys. Chem. Chem. Phys.* **2006**, *8*, 2499.
(19) O'Neil, M. P.; Wasielewski, M. R.; Khaled, M. M.; Kispert, L. D. *J. Chem. Phys.* **1991**, *95*, 7212.
(20) Bautista, J. A.; Connors, R. E.; Raju, B. B.; Hiller, R. G.; Sharples, F. P.; Gosztola, D.; Wasielewski, M. R.; Frank, H. A. *J. Phys. Chem. A* **1999**, *103*, 8751.
(21) Zigmantas, D.; Polívka, T.; Hiller, R. G.; Yartsev, A.; Sundström, V. *J. Phys. Chem. A* **2001**, *105*, 10296.

(22) Zigmantas, D.; Hiller, R. G.; Yartsev, A.; Sundström, V.; Polívka, T. *J. Phys. Chem. B* **2003**, *107*, 5339.
(23) Frank, H. A.; Bautista, J. A.; Josue, J.; Pendon, Z.; Hiller, R. G.; Sharples, F. P.; Gosztola, D.; Wasielewski, M. R. *J. Phys. Chem. B* **2000**, *104*, 4569.
(24) Vaswani, H. M.; Hsu, C.; Head-Gordon, M.; Fleming, G. R. *J. Phys. Chem. B* **2003**, *107*, 7940.
(25) Shima, S.; Ilagan, R. P.; Gillespie, N.; Sommer, B. J.; Hiller, R. G.; Sharples, F. P.; Frank, H. A.; Birge, R. R. *J. Phys. Chem. A* **2003**, *107*, 8052.
(26) Papagiannakis, E.; Larsen, D. S.; van Stokkum, I. H. M.; Vengris, M.; Hiller, R. G.; van Grondelle, R. *Biochemistry* **2004**, *43*, 15303.
(27) Papagiannakis, E.; Vengris, M.; Larsen, D. S.; van Stokkum, I. H. M.; Hiller, R. G.; van Grondelle, R. *J. Phys. Chem. B* **2006**, *110*, 512.
(28) Bürsing, R.; Lenzer, T.; Oum, K. *Chem. Phys.* **2007**, *331*, 403.
(29) *Handbook of Chemistry and Physics*, 85th ed.; CRC Press: Boca Raton, FL, 2004.
(30) Chen, Z.; Lee, C.; Lenzer, T.; Oum, K. *J. Phys. Chem. A* **2006**, *110*, 11291.
(31) Renge, I.; van Grondelle, R.; Dekker, J. P. *J. Photochem. Photobiol. A* **1996**, *96*, 109.
(32) He, Z.; Kispert, L. D.; Metzger, R. M.; Gosztola, D.; Wasielewski, M. R. *J. Phys. Chem. B* **2000**, *104*, 6302.
(33) Rückert, I.; Demeter, A.; Morawski, O.; Kühnle, W.; Tauer, E.; Zachariasse, K. A. *J. Phys. Chem. A* **1999**, *103*, 1958.
(34) Wohlfarth, C.; Wohlfarth, B. *Landolt-Börnstein - Vol. IV/6, Static Dielectric Constants of Pure Liquids and Binary Liquid Mixtures*; Springer: Berlin and Heidelberg, 1991.
(35) Wohlfarth, C.; Wohlfarth, B. *Landolt-Börnstein - Vol. III/38, Optical Constants*; Springer: Berlin and Heidelberg, 1996.
(36) Larson, E. J.; Pyszczynski, S. J.; Johnson, C. K. *J. Phys. Chem. A* **2001**, *105*, 8136.
(37) Frank, H. A.; Chynwat, V.; Desamero, R. Z. B.; Farhoosh, R.; Erickson, J.; Bautista, J. *Pure Appl. Chem.* **1997**, *69*, 2117.